Coupling Strength Distributions for Dynamic Interactions Experienced by Probe Molecules in a Polymer Host

Elizabeth A. Donley, Hermann Bach, Urs P. Wild, and Taras Plakhotnik*

Physical Chemistry Laboratory, Swiss Federal Institute of Technology, ETH-Zentrum, CH-8092, Zürich, Switzerland

Received: September 9, 1998; In Final Form: January 6, 1999

In this work, discrepancies between measured single-molecule linewidth distributions and distributions simulated with the standard tunneling model in the sudden-jump approximation are studied for terrylene and di-*tert*-butylterrylene dopant molecules in poly(vinylbutyral). The experimental data has been carefully checked for systematic errors. It is shown that the results are in disagreement with the standard model, but that the incorporation of a distribution of molecule−polymer coupling strengths would remove this disagreement. Additionally, the experimental observation of a surprising correlation between the single-molecule line areas and the matrix−molecule interaction strength is presented, and a hypothesis is put forward for its physical origin.

I. Introduction

In a glass, atoms or groups of atoms can be arranged in different spatial configurations. Even at very low temperatures, rather than the arrangements being frozen in, transitions between configurations occur by phonon-assisted tunneling. The two-level system (TLS) model fairly accurately describes many low-temperature properties of glasses that arise from these configurational changes .[1] The model was first proposed to explain anomalous thermal properties of amorphous solids at low temperatures[2,3] and was later applied to acoustic measurements and dephasing of optical transitions. In this study, we investigate the adequacy of the theory for modeling linewidth distributions measured with single-molecule spectroscopy (SMS).

A TLS can be mathematically modeled as a particle in a nearly symmetric double well potential. Transitions between the two lowest energy states (linear combinations of the two localized states) occur by tunneling through the barrier, where the energy difference between the two states is compensated by the creation or annihilation of phonons. The tunneling rate between the two states depends on the temperature, the asymmetry Δ, the tunneling splitting $J \propto e^{-\lambda}$, as well as on material constants affecting the phonon modes. The size of the splitting strongly depends on the tunneling parameter $\lambda = (2mVd^2/\hbar^2)^{1/2}$, which indicates the overlap of the wave functions. V is the barrier height between the two minima, d is the distance between them in configurational space, and m is the effective mass of the tunneling particle. Within the standard model, the distribution for λ is assumed to be flat over the relevant range of values, and because of the exponential dependence on λ, there is a broad distribution of tunneling splittings J.

TLS flips cause the transition frequencies of probe molecules doped into the glass to undergo spectral diffusion. In many previous papers on TLS dephasing of optical transitions, attention has been focused on the effect of TLS parameter distributions on the time and temperature dependence of chromophore transition frequencies (see for example refs 4−6), and less emphasis has been placed directly on the TLS−chromophore interaction mechanism, which is one of the main subjects considered here.

In this work, the simulated and measured linewidth distributions for single terrylene and di-*tert*-butylterrylene (DTBT) molecules in poly(vinylbutyral) (PVB) are compared. The agreement between measured linewidth distributions and theoretical distributions predicted with the standard tunneling model has so far been marginal,[7] with a few recurring discrepancies: experimental distributions are generally broader than those predicted by theory, and there are usually more narrow linewidth molecules measured than predicted.

Linewidth distributions are measured using single-molecule microscopy. The experimental bias toward measuring narrow linewidth molecules due to their brightness is investigated and circumvented by searching for peaks in the integrated intensities rather than the peak intensities. Additionally, the experimental discovery of a correlation between the single-molecule line areas and the linewidths is presented, which indicates that there is a parameter simultaneously affecting both quantities. Possible physical origins of this correlation are examined in detail.

II. Single Molecule−TLS Coupling

At any point in a glass, the total electric and strain fields are influenced by many TLSs, and the time-dependent transition frequency of a guest SM can be written as

$$\omega(t) = \omega_0 + \sum_j \theta_j(t) v_j \tag{1}$$

where $\theta_j = 0$ ($\theta_j = 1$) indicates that the jth TLS is in its ground (excited) state, and

$$v_j = 2\pi\alpha\eta_j/r_j^3 \tag{2}$$

is the frequency shift induced by excitation of the jth TLS. α, η_j, and r_j are the TLS−chromophore coupling constant, the relative orientation parameter, and the TLS−chromophore

* Corresponding author. Fax: +41 1 632 1021. E-mail: donley@phys.chem.ethz.ch or taras@phys.chem.ethz.ch.

10.1021/jp983653z CCC: $18.00
Published on Web 02/24/1999

distance for the *j*th TLS, respectively. In the standard model, α is assumed to be the same for all TLS−SM pairs.

The theory is largely phenomenological because very little is known about the microscopic nature of TLSs; however, there is reasoning behind eqs 1 and 2. The TLS−SM interaction is assumed to be dipolar, having a $1/r^3$ distance dependence. Usually, the interaction is said to arise from "elastic" dipole TLSs, whose flips cause mechanical strain fluctuations.[8] The effect of their flips on the chromophore frequency is like a pressure effect, which has been studied extensively with hole-burning techniques.[9] The mechanical displacements are thought to cause density fluctuations in the vicinity of the chromophores, affecting the magnitude of the dispersion interaction contribution to the shift of the transition frequency. Also, if the matrix is polar, elastic dipole flips may cause a shift of charges and permanent dipoles in the matrix, which may also cause energy shifts. The TLS−SM interaction could also originate from purely "electric" dipoles if the two states of the TLSs have different electric dipole moments. Then a TLS state flip itself can cause Stark shifts of the chromophore without displacement of the matrix. The TLS−SM coupling is actually a sum of electric and elastic dipole contributions.

It has been shown that the electrostatic contribution to the static guest−host interaction is roughly 2−3 orders of magnitude smaller than the dispersive contribution for octaethylporphin in polystyrene.[10] In addition, our measurements of the absorption spectra of terrylene in different polymer matrices (polyethylene (PE), poly(methyl methacrylate) (PMMA), polystyrene, polyisobutylene, and PVB) show that the solvent shifts for terrylene in polar and nonpolar matrices are similar in size. In fact, the deviations in the absolute wavelength of the shifted lines from host to host are much smaller than the inhomogeneous bandwidths. Therefore, the dispersion interaction contribution to the solvent shift seems to be much larger than the electrostatic contribution even for polar hosts. In spite of this, the electric dipole contribution to the dynamical coupling constant can be quite large or even dominant, because unlike a static shift, it is not averaged when a probe molecule interacts with many TLSs.

It has been shown that the Stark effect for single terrylene molecules in PE is linear because the molecular symmetry is broken by the matrix.[11] Therefore, the magnitude of the frequency shifts caused by electrostatic interactions between a SM and a fluctuating TLS is directly proportional to the local electric field. The electric dipole contribution to the coupling constant from eq 2 can then be estimated as

$$\alpha = \frac{1}{4\pi\epsilon\epsilon_0} L_c \Delta\mu_{TLS} \Delta\mu_{SM} \tag{3}$$

where $\Delta\mu_{TLS}$ is a dipole moment difference caused by a TLS flip, $\Delta\mu_{SM}$ is the dipole moment change of the chromophore under a transition from the ground to the excited state, ϵ is the dielectric constant, and $L_c = (\epsilon + 2)/3$ is the Lorentz local field factor (a topic of discussion in section VI). According to recent hole-burning measurements,[12] the TLSs in PMMA have an average dipole moment difference between the two TLS states of 0.4 D. The average induced dipole moment change for terrylene in PE has also been measured and is ~2 D[11] (a factor of 2 higher than the average modulus of the projection along the electric field). Using these values and $\epsilon = 2.84$ for PMMA[13] gives $\alpha \simeq 70$ GHz nm^3 as a rough estimate for the coupling constant. $\Delta\mu_{SM}$ strongly depends on the host[14] and is probably larger in PMMA than in PE since PMMA is polar. Anyhow, the above estimate for α is between the values estimated by Geva and Skinner for terrylene in PE (12 GHz nm^3) and in PMMA (190 GHz nm^3),[7] which are also only rough estimates because they depend on the values for the TLS densities which are only approximately known. Phonon echo measurements have also shown that there is an intrinsic electric dipole moment of tunneling systems even in undoped silicon of about 0.6 D.[15]

An additional factor of Δ_j/E_j is often included in eq 2, where Δ_j is the asymmetry parameter and $E_j = (\Delta_j^2 + J_j^2)^{1/2}$ is the TLS energy splitting. This factor is intuitively reasonable, since if the asymmetry Δ_j is equal to zero there will be no dipole moment difference between the two states of the TLS and the interaction strength will be zero. However, in the theoretical derivation of this factor,[1] several assumptions and approximations are made. Our simulations show that the inclusion of this factor does not produce a difference in the results of the simulations on a statistically significant level.

Normally, the coupling parameter α is treated as a constant in the simulations, but as is written in eq 3, it is a product of several parameters. There are two distinct types of parameters affecting the TLS−SM interaction: those explicitly connected to the probe molecules, which we refer to as inhomogeneous parameters, and those associated with the bath of TLSs, which we call homogeneous. Each SM has unique values for $\Delta\mu_{SM}$ and L_c which affect the interaction strength of the SM with the entire bath of TLSs, but each TLS may have a different $\Delta\mu_{TLS}$, η, and r. One can group all parameters into the single parameter $\Lambda = \Delta\mu_{SM} L_c \Delta\mu_{TLS} \eta / r^3$, which describes the TLS−SM interaction. The probability distribution for Λ for each molecule is simply

$$P_\Lambda(\Lambda) = \frac{4\pi}{3} \frac{\Delta\mu_{SM} L_c \rho_{TLS} \langle|\eta \Delta\mu_{TLS}|\rangle}{\Lambda^2 N_{TLS}} \tag{4}$$

which is proven mathematically in the Appendix. ρ_{TLS} is the TLS density and N_{TLS} is the number of TLSs considered. This depends on the upper distance cutoff r_{max}, which must be large enough for the SM line shapes to reach asymptotic values. Thus, the distributions of the homogeneous parameters η, $\Delta\mu_{TLS}$, and r can simply be replaced by average values in the simulations without changing the resulting distribution of SM line shapes.

III. Experimental Method

Either terrylene or DTBT molecules were codissolved with PVB in dichloromethane. The solutions were filtered with solvent resistant filters (Gelman Sciences, 0.45 μm pore size, Acrodisc PTFE filters) and either spin-coated or cast onto microscope cover slips. The samples were then baked under vacuum for several hours at ~80 °C, which is slightly above the glass transition temperature for PVB. The samples had final chromophore concentrations of $\sim 10^{-6}$ M and thicknesses of ~1 μ m. The thicknesses were determined using an atomic force microscope to measure the depth of a scratch made through the sample. We could not observe SMs in samples thinner than ~200 nm, presumably because of surface broadening effects.[16] All of the measurements were performed with a sample temperature of 1.8 K.

The data were collected using single-molecule microscopy,[17−19] which has the advantage that many molecules from different areas of the sample are observable in parallel under identical experimental conditions. The laser wavelength was in the range from 571 to 575 nm, which is on the red edge of the inhomogeneous band for both terrylene and DTBT in PVB, whose inhomogeneous absorption bands are centered at 565 nm. Circularly polarized laser light was used to excite the molecules, which lessens the preference for measuring molecules with

dipole moments parallel to any given direction. All molecules (except for the intensity-ramped terrylene measurements presented in section IV) were measured with intensities below 50 mW/cm^2. 100 mW/cm^2 is the saturation intensity for terrylene in PE.[20] The saturation intensities for terrylene and DTBT in PVB should be much higher since the typical linewidths are about four times broader in PVB than in PE.[21] Digitized fluorescence images of the sample were collected at a series of excitation frequencies, resulting in three-dimensional data cubes having one frequency and two position coordinates,[19] from which fluorescence-excitation spectra for single molecules (SMs) were extracted. Since the data was usually quite noisy, the SM search procedure is a critical step in the data analysis so it is described in detail below.

Each data cube contained from six to eight 500-image scans of the same 10 GHz frequency range so that the reproducibility of SM features could be assessed. To search the huge data files (~1 GB) for SMs, the six to eight scans were first summed up into a single scan. Then a 1 GHz running average in the frequency dimension was performed. This procedure roughly equalizes peak intensity values to the integrated line intensities, which in principle should be the same for broad and narrow linewidth molecules. Searching for peaks in the integrated intensity is therefore less biased than searching for absolute maxima, which favors narrow linewidth molecules since they are on average brighter. This point is further discussed in section IV. A compressed sample image was then formed by taking the difference between the maximum and minimum intensities for each *x*,*y* point in the averaged data. Peaks were then found in the compressed image.

Frequency trajectories for each of the frequency scans were then extracted from the data at the *x*, *y* coordinates of the peaks in the compressed image. The features having amplitudes of at least double the variance of the noise which were also observed repeatedly were counted as single molecules. For a simple characterization, the SM line shapes were fit with Lorentzians, which gave good estimates for the full width at half-maximum even though the individual line shapes were not Lorentzians. The whole data handling and analysis procedure took several hours on a SPARC 5 workstation for each experiment.

IV. Linewidth Distributions

Shown in Figure 1 are six measured (a−f) and six simulated (g−l) fluorescence-excitation spectra of DTBT molecules in PVB. The Lorentzian fits are also shown. The measured spectra are averages of eight consecutive 20 s scans and have been selected at random from the list of DTBT molecules. Simulations are performed following the procedure recently described by Geva and Skinner,[7] with the exception that noise was added to the spectra and they were fit to Lorentzians. The same standard distributions for Δ and J were used. To reduce the time of the calculations, simplifications can also be implemented. We found that to a very high degree of accuracy, linewidth distributions calculated at different values of α were identical within a scaling factor. This follows from the simplified expression for the dipole autocorrelation function presented by Pfluegl et al.[22] The noise level on the SM spectra was characterized for all 919 of the molecules by taking the difference between the raw spectra and the Lorentzian fits and dividing the noise into two components. The peak contribution scaled by the signal intensity has an average value of 37% of the peak height at the maximum, and the background noise level is roughly constant for all molecules and equals 20% of the average peak height. The noise on the simulated spectra has two components which were chosen to match the measured noise levels.

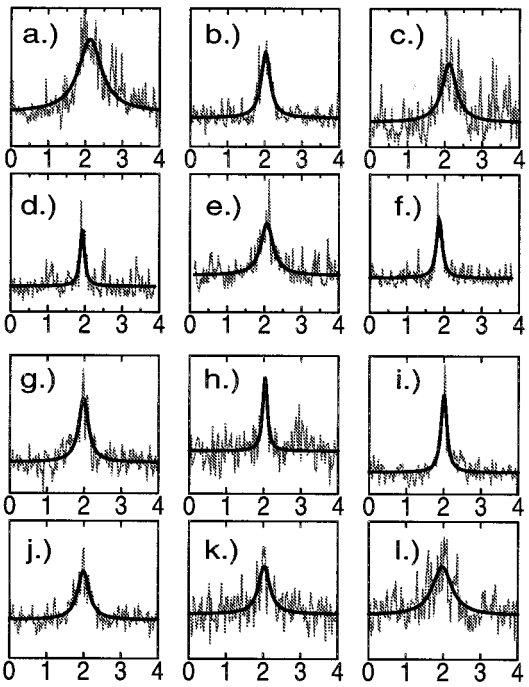

Figure 1. Measured (a−f) and simulated (g−l) fluorescence-excitation spectra of single DTBT molecules in PVB, shown with Lorentzian fits. The horizontal axes are the frequency in GHz and the vertical axes are intensity in arbitrary units. Random noise was added to the simulated spectra (see text).

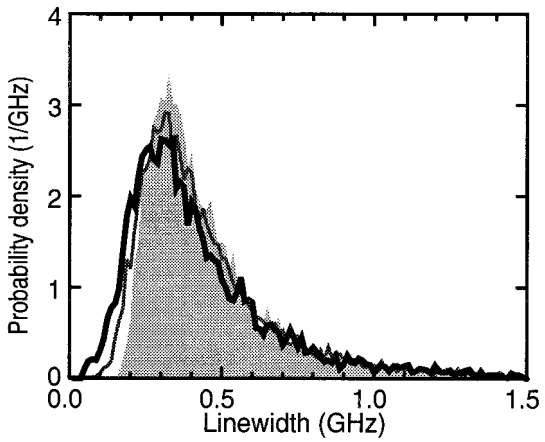

Figure 2. Examples of simulated linewidth distributions. The narrowest distribution (shaded) was simulated without adding noise to the spectra. The thin-lined distribution had an added peak noise level of 37% of the peak height (to match the noise level on the measured spectra) and was about 10% broader than the noiseless distribution. The broadest distribution had a noise level of 55% of the peak height and was 15% broader and more symmetric than the noiseless distribution.

Adding noise broadens the linewidth distribution, which is is illustrated in Figure 2. Three simulated linewidth distributions having different noise levels are shown. The narrowest distribution has no added noise. The other two distributions were simulated with peak (background) noise contributions of 37% (20%) and 55% (30%). The distributions with added noise are 10% and 15% broader than the noiseless histogram for the peak noise levels of 37% and 55%, respectively.

Figure 3a is a histogram of measured linewidths for 919 DTBT molecules in PVB. The statistics are improved over the previously measured histogram of terrylene in PVB,[23] with more

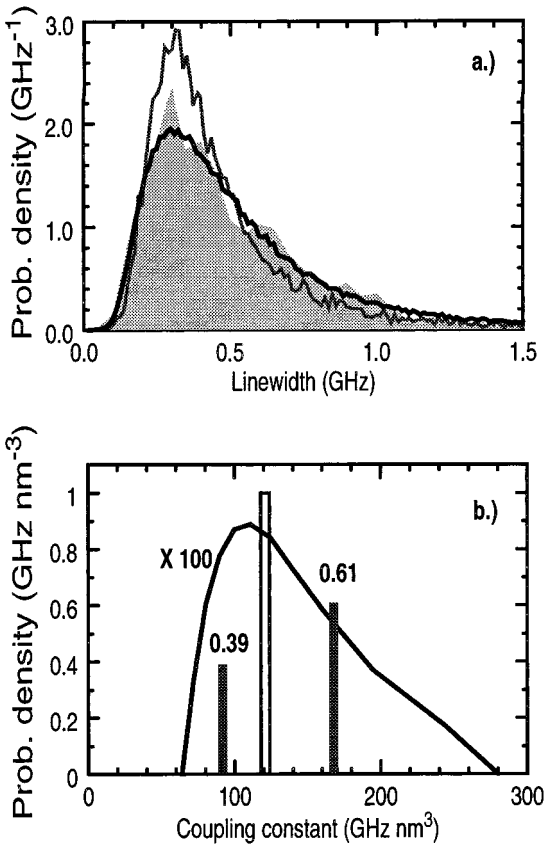

Figure 3. (a) DTBT data with a fit to a single coupling constant. Also shown is a fit to an α distribution. The confidence intervals for the fits to a single α and a smooth α distribution are 10^{-7} and 50%, respectively. (b) The α distribution found from fitting the data in (a). The hollow vertical bar shows the value for the best fit of a single α (121 GHz nm^3). The two filled vertical bars show a bimodal distribution (92 and 168 GHz nm^3) that fits the experimental distribution with a confidence interval of ~30%.

than 4 times as many molecules measured. A simulated fit to the data is shown, produced by finding the best fit using the TLS−chromophore coupling strength (α in eq 2) as an adjustable fit parameter in the simulations, which gives a value of α = 121 GHz nm^3. A fit to a coupling constant distribution is also shown, which is discussed in section V. The distributions containing 1600 molecules were normalized to the number of measured molecules for the fitting procedure.

The agreement between the two distributions may not look so bad, but in fact it is highly unlikely that the two distributions were sampled from the same parent distribution considering the number of molecules measured in the experiment. To obtain a quantitative measure for the dissimilarity between the two distributions, we have analyzed the disagreement statistically by calculating χ_ν^2 for a goodness-of-fit estimation,[24] where

$$\chi_\nu^2 = \frac{1}{\nu}\sum_{i=1}^{N}\left(\frac{1}{\sigma_i^2}[y_i - y(x_i)]^2\right) \tag{5}$$

The y_i are the bin heights for the measurements and the $y(x_i)$ are the heights of the simulated bins. ν is the number of degrees of freedom. For comparing the distributions in Figure 3, $\nu = N - 2$, where N is the number of bins, owing to the fact that there is one adjustable fit parameter (α) and a constraint for the normalization. Assuming that the molecular counting procedure obeys Poissonian statistics, the uncertainty for each point is the square root of the number of molecules in the bin. σ_i in eq 5 includes the uncertainties of both distributions added in quadrature. This gives $\chi_\nu^2 \simeq 3.6$ ($\nu = 22$). According to the probability distribution for χ_ν^2, the probability that the two distributions were sampled from the same parent distribution (the confidence interval) is approximately 10^{-7}.[24] The confidence intervals are very sensitive to the noise level. When noise was not added to the simulated spectra, the probability was only 10^{-12}. The best agreement was found when the noise level was increased to 55% on the peak and 30% on the background (50% more noise than on the experimental spectra), where the probability increased to 0.2%. As the noise was further increased, the confidence interval decreased because the simulated distributions became more symmetric and could no longer reproduce the sharp experimental linewidth cutoff at the natural linewidth.

Since the theory and experiment were in such poor agreement, we changed the probe molecule to terrylene, for which there was already a published linewidth distribution,[23] and a more thorough investigation into possible systematic errors was performed, beginning by considering the emission rates. Well below saturation, since the saturation intensity for a single molecule is proportional to the linewidth Γ,[25] the emission rate is

$$R(I) = R_\infty \frac{I}{I_S} \propto R_\infty \frac{I}{\Gamma} \tag{6}$$

Since the rate is inversely proportional to Γ, the single-molecule line amplitudes and hence the signal to noise ratios should be smaller for broad-linewidth molecules.

This could create a bias toward measuring narrow lines if the line amplitudes for the broad molecules are insufficient to distinguish them from the noise. To reduce this possible bias, the broader linewidth molecules can be measured at higher intensity since the photo count rate goes up linearly with intensity while the shot noise is proportional to the square root of the rate. Since their saturation intensity is larger, there should be no saturation broadening as long as I/Γ is below I_{S_0}/Γ_0, where Γ_0 is the lifetime-limited linewidth and I_{S_0} is the saturation intensity for molecules with lifetime limited linewidths.

The total integrated emission from a SM should be independent of the linewidth. Below saturation, the total number of photons emitted by a single molecule during a scan is proportional to the area under the SM line profile. Ignoring the phonon wing, the area is

$$A = R\Gamma \propto R_\infty I \propto \Omega_R^{\,2} \tag{7}$$

which follows from eq 6. Ω_R is the Rabi frequency, which specifies the strength of the coupling between the SM and the electric field. This relation is further discussed at length in sections VI and VII.

To test if the measured linewidth distributions are intensity dependent, the distribution of linewidths was measured at three linearly increasing intensities: 50, 100, and 150 mW/cm^2. The molecule search was based on the line area discrimination procedure described in section III. The confidence intervals for the agreement between the three resulting linewidth distributions are 95%, 75%, and 75% for the low and medium intensity, the medium and high intensity, and the low and high intensity measurements, respectively. Since these three distributions are statistically indistinguishable, they can be combined into the single distribution with 486 molecules that is shown in Figure 4. The confidence interval for the agreement between the distribution and a fit to a single α (α = 154 GHz nm^3) is

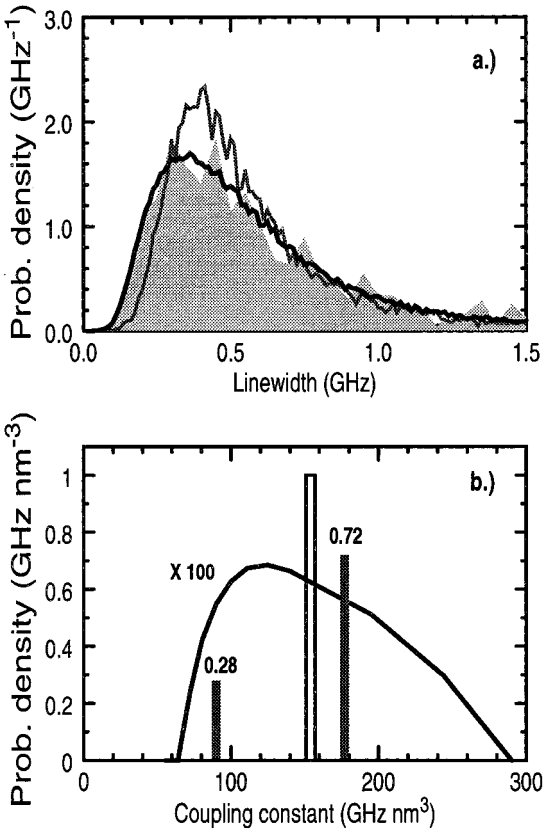

Figure 4. (a) Terrylene data with a fit to a single coupling constant α. Also shown is a fit to an α distribution. The confidence intervals for the fits to a single α and a smooth α distribution are 0.2% and 65%, respectively. (b) The α distribution found from fitting the data in (a). The hollow vertical bar shows the value for the best fit of a single α (154 GHz nm^3). The two filled vertical bars show a bimodal distribution (90 and 177 GHz nm^3) that fits the experimental distribution with a confidence interval of ∼30%.

∼0.2%. Interestingly, there is less line broadening for DTBT than there is for normal terrylene.

We have statistically compared the combined distribution with the distribution measured by Kozankiewicz et al.,[23] and we get $\chi_\nu^2 \simeq 3.9$ (ν=10), which has a confidence interval of approximately 0.01%. The peak in Kozankiewicz' distribution is shifted to larger linewidths. The distribution could depend on the sample preparation technique. Kozankiewicz et al. used acetone as a solvent for sample preparation, and they did not bake the samples to remove the excess solvent, which may cause additional line broadening.

V. Fitting the Data to a Coupling Constant Distribution

Owing to the fact that the TLS−SM coupling parameter α includes factors for the induced SM dipole moment $\Delta\mu_{SM}$ and the local field factor L, both of which are inhomogeneous parameters, it may be necessary to include a distribution for α in the simulations. This is a main topic of discussion in section VII. Rather than fitting the experimental distributions to single α, as was done in section IV, they can be fit using a model modified to include an α distribution. For the fit, a series of M distributions is calculated for M different TLS−SM coupling constants α. The distributions with larger α are broader and the peak positions are shifted to larger linewidths. A linear combination of these distributions is fit to the experimental distribution.

The M calculated distributions are broken into N bins and expressed vectorally as $\vec{D}_m = [D_{m1}, D_{m2}, .., D_{mN}]$, the index m running from 1 to M. The experimental distribution is broken into the same bins and expressed as $\vec{Y} = [Y_1, Y_2, ..., Y_N]$. A vector of probabilities for the M coupling constants $\vec{P} = [P_1, P_2, ..., P_M]$ is found such that the function

$$\chi_\nu^2 = \frac{1}{\nu}\sum_{n=1}^{N}\frac{(Y_n - \sum_{m=1}^{M} D_{mn}P_m)^2}{\sigma_n^2} \qquad (8)$$

is minimized. χ_ν^2 is the same function that we discussed previously when comparing linewidth distributions. There are two restrictions applied to the probability vector $\vec{P}$: all of the entries must be nonnegative and the vector must be smooth. To fulfill the nonnegativity requirement, the minimum is found within the volume of the vector space with nonnegative probabilities. To fulfill the smoothness requirement, the α distribution is smoothed as much as possible while still being within the range of the statistical uncertainty of the experimental distribution. It is assumed that the distribution is perfectly smooth when each point in the curve is the average of its two neighboring points.

The histograms simulated with α distributions are shown with the experimental data in Figures 3a and 4a. The α distributions themselves are shown in Figures 3b and 4b. For the calculation of χ_ν^2, again we need to know the number of degrees of freedom. In this case ν is not as well-defined, since there is not a clear number of parameters in the fitting procedure. However, using an α distribution is like generating an additional parameter for the width of the distribution, and perhaps another for the asymmetry. We therefore have three parameters—the mean, the width, and the asymmetry. The normalization is an additional constraint. We therefore assume that $\nu = N - 4$. Therefore, the α distribution fits have confidence intervals of 55% ($\chi_\nu^2 = 0.92$, $\nu = 21$) for DTBT and 65% for terrylene ($\chi_\nu^2 = 0.85$, $\nu = 21$).

Both linewidth distributions can also be reasonably fit with a simple sum of the two coupling constants that are shown as filled vertical bars in the α distributions with confidence intervals of ∼30% in both cases. The best fits for a single coupling constant α are also shown as hollow vertical bars. The α distribution for the best fit to the data always has a complex structure, but there is no reason to believe that the structure is real given the statistical uncertainty of the data. The smoothness requirement eliminates this structure without significantly altering the mean and width of the distribution.

The linewidth distribution depends on the product of the coupling constant and the TLS density; thus the distributions in Figures 3b and 4b could also be caused by a fluctuation of the TLS number interacting with the probe molecules, which follows directly from eq 4. These fluctuations, however, would have to be much larger than Poissonian fluctuations, which are already included in the theory containing a single coupling constant since the TLSs randomly distributed in space.

Actually, a distribution of coupling parameters should not come as a surprise, knowing that the chromophore transition frequency is inhomogeneously broadened. The inhomogeneous broadening indicates that there is a distribution of static coupling constants. Our results seem to indicate that there is a distribution of dynamic coupling as well.

VI. Linewidth−Line Area Correlation

The relationship in eq 7 predicting that the line areas should be independent of the linewidths was checked by making a

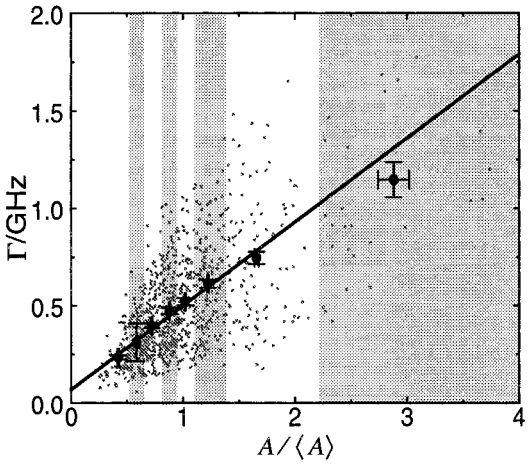

Figure 5. The linewidth vs the normalized line area for the DTBT data from Figure 3.

scatter plot of the linewidths vs the areas under the SM curves. Figure 5 is such a plot for the DTBT molecules in PVB from the histogram in Figure 3. The line area A was normalized to the average area for each data set independently, since the detected emission varies from day to day due to laser power changes, detection efficiency fluctuations, etc. There is a clear correlation between the linewidths and the line areas. We have observed this correlation in most other systems checked, including terrylene in PE, *n*-alkanes, and PVB. The correlation, however, does not appear for terrylene in naphthalene crystals, where the linewidth distribution is narrow and the molecules are very stable.

The correlation coefficient for a simple linear regression to the data is 0.67. The cone shape is caused by two factors: a distribution of the relative orientation of the SMs with respect to the laser polarization causing an area distribution for a given linewidth, and spectral diffusion, which causes a linewidth distribution for a given area. For example, assuming no spectral diffusion and perfect intrinsic correlation $A = k\Gamma \sin^2\theta$, where k is the slope of the correlation. For a random distribution of orientations, the correlation coefficient would be 0.75.

A linear regression does not appear to fit the data well though, because too much weight is given to the points for large Γ where the scatter is large. To do a weighted fit, the average values for the points within the $A/\langle A\rangle$ ranges given by the shaded areas in Figure 5 were calculated, which contain an approximately equal number of data points. The solid line is a weighted linear fit to the averaged points, found using the uncertainties in the linewidths as weighting factors. The slope of the fit is 430 MHz and the y intercept is 70 MHz. The magnitudes of these values and their significance are discussed in the next section. We have observed that the slope decreases due to saturation as the power is further increased, but we see no saturation up to the intensity of 150 mW/cm^2.

VII. Discussion

The correlation shown in Figure 5 is an experimental fact. Here we begin to hypothesize about its cause, which we think is related to the disagreement between measured linewidth distributions and simulations in which a single coupling constant is used.

First, we would like to dismiss photoinduced spectral diffusion as the cause of the correlation in Figure 5. Note that the areas and not the emission rates are represented on the x-axis. The correlation therefore has the effect of somewhat evening out the emission rates for broad and narrow lines, but on average the narrow lines still have higher amplitudes (molecules with equal amplitudes lie on a straight line through the origin.) Therefore, the power dissipated to the matrix upon excitation is on average greater for the narrow lines, which undergo less spectral diffusion.

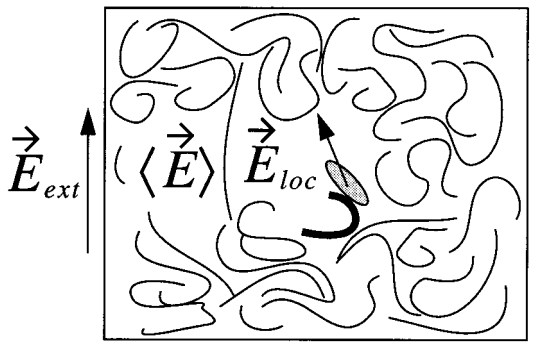

Figure 6. Electric fields inside and outside of the sample. The local field at the position of the chromophore is strongly influenced by nearby perturbers.

We also do not think that the correlation is related to the phonon wing. In eq 7, the contribution from the phonon wing to the line area was neglected. The relative area of the zero phonon line to the phonon wing is characterized by the Debye−Waller factor $\kappa(T)$, which depends on the electron−phonon coupling and the temperature. The phonon wing is usually 10^3−10^4 times broader than the zero phonon line[26] and cannot be observed in SM spectra. At liquid ^{4}He temperatures, $\kappa(T)$ is ~0.5 or higher for systems that are good for SMS. If $\kappa(T)$ varies and increases with the linewidth, this could conceivably cause the correlation seen in Figure 5, but we cannot think of any reason why $\kappa(T)$ should be larger for broad lines. If anything, it should be larger for the narrow lines, since it increases in more-ordered systems where there is less spectral diffusion.[27]

The more likely source for the correlation is the effective transition dipole moment, or equivalently, the local field factor, which is an old but still unsettled issue.[28,29] The Rabi frequency of the probe molecule is

$$\Omega_R = \frac{\vec{\mu}_A \cdot \vec{E}_{loc}}{\hbar} = \frac{\vec{\mu}_A \hat{L} \langle \vec{E} \rangle}{\hbar} \tag{9}$$

where $\langle \vec{E} \rangle$ is the macroscopic field in the medium, which is reduced from the externally applied laser field by surface reflections. $\vec{\mu}_A$ is the transition dipole moment of the chromophore in free space. The factor $\hat{L}$ can be viewed as changing the transition dipole moment into the effective transition dipole moment $\vec{\mu}_{eff} = \vec{\mu}_A \hat{L}$. In the traditional literature it is usually visualized as a field enhancement,[30] where $\vec{E}_{loc} = \hat{L}\langle \vec{E} \rangle$ is the local field present inside a small cavity in the dielectric containing the SM, which is magnified by the polarization of the medium induced by the laser field. In the simplest case of considering a continuous, homogeneous, isotropic medium

$$\hat{L}_c = \hat{L}_c \hat{I} = \frac{\epsilon + 2}{3} \tag{10}$$

where $\hat{I}$ is the unit matrix and ϵ is the dielectric constant of the medium. $\epsilon = 2.7$ for PVB.[13] The subscript c indicates that this estimate comes from an isotropic continuum approximation.

Figure 6 illustrates a model of the microscopic host geometry surrounding a chromophore. The polymer chains are represented by curved lines. Far from the chromophore, the sample appears continuous because the number of chains becomes large. The

influence of this part of the sample can be well described by eq 10. However, on a nanometer scale the concept of ϵ does not hold, and the contribution from the nearby chains must be treated differently. On the size scale of a single molecule (~1 nm), the dielectric is neither isotropic nor homogeneous, and therefore a distribution of L factors is expected.

The L factor distribution can be roughly estimated from the data by taking the square root of the line areas and normalizing the mean value to L_c. Doing this, one gets a relative width of the L factor distribution of $\Delta L_{FWHM}/\langle L\rangle$ ~50%, which is only an upper bound since the relative angular orientation between the laser polarization and μ_A also causes a distribution of line areas, but one can then estimate the lower bound for the average distance between the SM and the polarizable object perturbing its transition dipole moment.

Strictly speaking, L is an average over the spatial volume occupied by an optical electron, but the effective dipole moment of a chromophore A in the presence of a polarizable object B can be approximated by[31]

$$\vec{\mu}_{eff} = \vec{\mu}_A - \hat{\alpha}\frac{3(\vec{\mu}_A\cdot\hat{n})\hat{n} - \vec{\mu}_A}{R^3} \qquad (11)$$

$\hat{\alpha}$ is the polarizability tensor of the object B, R is the distance between A and B, and $\hat{n}$ is the unit vector pointing from A to B. The second term originates from the induced dipole in the object B resulting from the dipole field of the molecule A. This equation holds for both transition dipole moments (ac fields) and permanent dipole moments (dc fields), but $\hat{\alpha}$ may be different for the two. It has been found from *ab initio* calculations that a PVB monomer unit has a dc polarizability of ~15 Å^3.[32] In transparent solid samples, the polarizability values do not change much between dc and optical frequencies, and therefore both fields are similarly affected by nearby polarizable objects.

When $\vec{\mu}_A$ is collinear with $\hat{n}$, the effective dipole is reduced by the factor $2\hat{\alpha}\vec{\mu}_A/R^3$. When $\vec{\mu}_A$ is perpendicular to $\hat{n}$, $\vec{\mu}_{eff}$ is increased by $\hat{\alpha}\vec{\mu}_A/R^3$. Therefore, the effective local field factor should be $L_c(1 - 2\hat{\alpha}/R^3)$ when B is at the poles of $\vec{\mu}_A$ and $L_c(1 + \hat{\alpha}/R^3)$ when B is at the equator of $\vec{\mu}_A$. L_c takes into account the contribution from the continuum-like part of the sample far from the chromophore and can be found from eq 10. With these limits, one must assume $R \sim 5$ Å if $\Delta L_{FWHM}/\langle L\rangle = 0.5$. The length and width of terrylene molecules are roughly 13.5 and 6.7 Å, respectively.[33] The thickness estimated from the intermolecule spacing for crystallized perylene molecules is approximately 3.5 Å.[34] The necessary distances are therefore about the size of the molecular dimensions. A larger L factor strengthens both the SM−laser field coupling and the SM−TLS coupling, causing both a higher emission rate and stronger diffusional broadening. This can explain the correlation seen in Figure 5.

One interesting consequence of eq 11 is that there should be a distribution of natural lifetimes T_1 among the molecules, since $T_1 \propto 1/|\vec{\mu}_{eff}|^2$.[35] Perturbations to the natural lifetime as large as 10% for 9,10-dichloroanthracene−inert gas heteroclusters have been observed in experiments and examined theoretically.[36] The polarizabilities of inert gas atoms are roughly an order of magnitude smaller than the polarizabilities of PVB monomers, so this effect can be larger in PVB. The $1/2\pi T_1 = \Gamma_0$ contribution to the linewidth is small compared to the diffusional broadening except for a few of the narrowest molecules, so it is not necessary to include variations of T_1 in the simulations. The only published value for T_1 is for terrylene in PE and is 3.78 ± 0.03 ns. This gives $\Gamma_0 = 42$ MHz.[37]

Now we can analyze the slope of the correlation curve in Figure 5. The abscissa represents the normalized area of the SM lines, which according to eqs 7 and 9 is equal to the normalized square of L, $X = L^2/\langle L^2\rangle$. If we assume that $\Gamma = f(\xi)L + \Gamma_0$, where $f(\xi)$ is independent of L but depends on a large number of other variables like the TLS parameters, then the linewidth should roughly go as the square root of the normalized area, but we observe rather a linear dependence. The linewidth could be proportional to L^2 if $\Delta\mu_{SM}$ is also proportional to L. In this case, $\Gamma = f(\xi)L^2 + \Gamma_0$, and for the averaged points in Figure 5

$$Y_i = \langle\Gamma\rangle_b X_i + \Gamma_0 \qquad (12)$$

where $\langle\Gamma\rangle_b$ is the average broadening contribution to the linewidth. This predicts a linear correlation with a slope of $\langle\Gamma\rangle_b = 499$ MHz for the molecules in Figure 5, in fair agreement with the experiment, where the slope is 430 MHz and the intercept is 70 MHz.

The microscopic origin of $\Delta\mu_{SM}$ is the local symmetry breaking around the probe molecule. $\Delta\mu_{SM}$ is proportional to the strength of the internal fields arising from the charge distribution in the matrix.[38] A possible origin of a linear correlation between L and $\Delta\mu_{SM}$ could be that these fields are also enhanced by the local field factor.

The existence of a distribution of local field factors is not a new idea. In a previous work, we used the concept to explain a discrepancy between measured and calculated saturation intensities for pentacene in *p*-terphenyl as well as the distribution of quadratic Stark shift coefficients in the same system.[25] In saturation experiments on seven single pentacene molecules in *p*-terphenyl, the projection of local field tensor onto the polarization of the laser light was estimated to be 2.1, with a relative width of the distribution $\Delta L_{FWHM}/\langle L\rangle = 50\%$. Since *p*-terphenyl is a crystalline host, the molecular orientations are not random and hence this value is not averaged over orientations.

Interestingly, we have also found that the correlation between the line areas and the linewidths exists even for a single molecule undergoing spectral diffusion. We have analyzed data from Mauro Croci's Ph.D. thesis[33] for a single terrylene molecule in *n*-hexadecane that was observable for a period of nearly 4 h and was scanned over 5000 times. The center absorption frequency fluctuated during this time as did the linewidth. The correlation was clearly visible and the slope decreased as a function of intensity. The correlation was not cone shaped, so the orientation of the molecule must have been preserved during the experiment. The distribution of local field factors for this molecule had a relative width of 15%. The spectral diffusion was photoinduced in this case, which must mean that the excitation of the molecule was causing structural changes in the local environment, in turn causing changes of the transition dipole moment.

VIII. Conclusions

Distributions of linewidths for terrylene and di-*tert*-butylterrylene molecules in poly(vinylbutyral) have been carefully measured with special attention paid to checking possible systematic errors. DTBT molecules undergo less spectral diffusion than do normal terrylene molecules, which may be a result of shielding from the matrix by the bulky *tert*-butyl groups, reducing either the induced dipole moment or the local field factor. Experimental results and simulations compared using the standard model in the sudden-jump approximation were in disagreement with each other. The agreement could be

greatly improved by adding noise to the simulated spectra, but the best agreement was found when the experimental distributions were fit to a modified version of the standard model that allowed for a distribution of TLS−SM coupling constants.

A correlation between the SM areas and linewidths has also been observed, which is an interesting result that has not been recognized with ensemble measurements like hole-burning and photon echoes. With photon echo decays, for example, it may be difficult to observe the nonexponentiality that would result from a distribution of lifetimes, particularly if the measurements do not span a large dynamic range.

This correlation has also been observed in many other systems that we have checked, including terrylene in *n*-dodecane, *n*-hexadecane, and polyethylene, and di-*tert*-butylterrylene in PVB, but the correlation was not clearly visible for terrylene in naphthalene crystals where there is very little disorder. This leads us to believe that the correlation is a universal property in amorphous hosts. One possible explanation for the correlation is that there is a distribution of effective transition dipole moments (or equivalently local field factors) caused by environmental inhomogeneities—a hypothesis which is also consistent with the shape of the linewidth distributions.

Acknowledgment. Fruitful discussions with Boris Kharlamov, Eitan Geva, Ernst-Udo Wallenborn, Gert Zumofen, Lothar Kador, and Felix Graf are gratefully acknowledged. We are also thankful to Prof. Müllen (MPI Mainz) for the gift of the alkylated terrylene. This work was funded by the ETH Zürich.

Appendix:

With $\Lambda = D\mu\eta r^{-3}$, where $\mu = \Delta\mu_{TLS}$ and $D = \Delta\mu_{SM}L_c$ and assuming $\mu\eta > 0$

$$P_\Lambda(\Lambda) = \int\int_{\eta\mu>0} P_{\eta\mu}(\eta,\mu)\,\mathrm{d}\eta\,\mathrm{d}\mu \int_0^{r_{max}} \delta(D\mu\eta r^{-3} - \Lambda) P_r(r)\,\mathrm{d}r \tag{A1}$$

where $P_{\eta\mu}(\eta,\mu)$ is the probability distribution for η and μ, and $P_r(r)$ is the probability distribution for r. The integral is nonzero only for $r_{max} > (D\eta\mu/\Lambda)^{1/3}$, which always holds if $r_{max} > (D\eta_{max}\mu_{max}/\Lambda)^{1/3}$. Integrating over r and substituting $P_r(r) = (3/r_{max}^3)r^2$

$$P_\Lambda(\Lambda) = \frac{D}{r_{max}^3\Lambda^2}\int\int_{\eta\mu>0} \eta\mu P(\eta,\mu)\,\mathrm{d}\mu\,\mathrm{d}\eta \tag{A2}$$

and finally

$$P_\Lambda(\Lambda) = \frac{D\langle|\eta\mu|\rangle}{r_{max}^3\Lambda^2} = \frac{4\pi}{3}\frac{D\rho_{TLS}\langle|\eta\mu|\rangle}{\Lambda^2 N_{TLS}} \tag{A3}$$

References and Notes

(1) Phillips, W. *Rep. Prog. Phys.* **1987**, *50*, 1657−1708.
(2) Anderson, P.; Halperin, B.; Varma, C. *Philos. Mag.* **1972**, *25*, 1−9.
(3) Phillips, W. *J. Low. Temp. Phys.* **1972**, *7*, 351.
(4) Esquinazi, P., Ed. *Tunneling systems in amorphous and crystalline solids*; Springer Verlag: Berlin, 1998.
(5) Narasimhan, L.; Littau, K.; Pack, D. W.; Bai, Y.; Elschner, A.; Fayer, M. *Chem. Rev.* **1990**, *90*, 439−457.
(6) Silbey, R.; Koedijk, J.; Völker, S. *J. Chem. Phys.* **1996**, *105*(3), 901−909.
(7) Geva, E.; Skinner, J. *J. Phys. Chem.* B **1997**, *101*, 8920−8932.
(8) Black, J.; Halperin, B. *Phys. Rev. B* **1977**, *16*(6), 2879−2895.
(9) Haarer, D. In *Persistent spectral hole-burning: Science and applications*; Moerner, W. E., Ed.; Springer-Verlag: Berlin, 1988; Chapter 3, pp 79−125.
(10) Kador, L.; Jahn, S.; Haarer, D.; Silbey, R. *Phys. Rev. B* **1990**, *41*(17), 12215−12226.
(11) Orrit, M.; Bernard, J.; Zumbusch, A.; Personov, R. *Chem. Phys. Lett.* **1992**, *196*,(6) 595−600.
(12) Maier, H.; Wunderlich, R.; Haarer, D.; Kharlamov, B.; Kulikov, S. *Phys. Rev. Lett.* **1995**, *74*(26), 5252−5255.
(13) Ku, C. C.; Liepins, R. *Electrical properties of polymers: chemical principles*; Hanser: Munich, 1987.
(14) Gerblinger, J.; Bogner, U.; Maier, M. *Chem. Phys. Lett.* **1987**, *141*(1,2), 31.
(15) Golding, B.; Schickfus, M.; Hunklinger, S.; Dransfeld, K. *Phys. Rev. Lett.* **1979**, *43*(24), 1817−1821.
(16) Fleury, L.; Gruber, A.; Dräbenstedt, A.; Wrachtrup, J.; von Borczyskowski, C. *J. Phys. Chem. B* **1997**, *101*, 7933−7938.
(17) Croci, M.; Irngartinger, T.; Renn, A.; Wild, U. *Exp. Techniques Phys.* **1995**, *41*(2), 249−257.
(18) Jasny, J.; Sepiol, J.; Irngartinger, T.; Traber, M.; Renn, A.; Wild, U. P. *Rev. Sci. Instrum.* **1996**, *67*(4), 1425−1430.
(19) Bach, H.; Donley, E. A.; Traber, M.; Renn, A.; Wild, U. P. *Opt. Mater.* **1998**, *9*, 376−380.
(20) Tchénio, P.; Myers, A. B.; Moerner, W. E. *J. Lumin.* **1993**, *56*, 1−14.
(21) Fleury, L.; Zumbusch, A.; Orrit, M.; Brown, R.; Bernard, J. *J. Lumin.* **1993**, *56*, 15−28.
(22) Pfuegl, W.; Brown, F. L. H.; Silbey, R. J. *J. Chem. Phys.* **1998**, *108*(16), 6876−6883.
(23) Kozankiewicz, B.; Bernard, J.; Orrit, M. *J. Chem. Phys.* **1994**, *101*(11), 9377−9383.
(24) Meyer, S. L. *Data analysis for scientists and engineers*; Wiley: New York, 1975.
(25) Plakhotnik, T.; Donley, E. A.; Wild, U. P. *Annu. Rev. Phys. Chem.* **1997**, *48*, 181−212.
(26) Orrit, M.; Bernard, J.; Brown, R.; Lounis, B. *Progress in Optics*; Elsevier: Asterdam, 1996, Vol. 35.
(27) Renge, I. *J. Chem. Phys.* **1997**, *106*(14), 5835−5849.
(28) Lagendijk, A.; Nienhuis, B.; van Tiggelen, B. A.; de Vries, P. *Phys. Rev. Lett.* **1997**, *79*(4), 657−660.
(29) Schuurmans, F. J.; de Lang, D. T.; Wegdam, G. H.; Sprik, R.; Lagendijk, A. *Phys. Rev. Lett.* **1998**, *80*(23), 5077−5080.
(30) Böttcher, C. *Theory of Electric polarization*, 2nd ed.; Elsevier: Amsterdam, 1973; Vol. 1.
(31) Liver, N.; Nitzan, A.; Amirav, A.; Jortner, J. *J. Chem. Phys.* **1988**, *88*(6), 3516−3523.
(32) Wallenborn, E.-U., unpublished work. The isotropic *ab initio* (CPHF RHF/6-31G*) polarizability of 4,6-dimethyl-2-propyl-1,3-dioxane is 14.4 Å^3. The Eigenvector with the largest Eigenvalue (16.4 Å^3) is roughly parallel to a line through the C(1)−C(4) atoms of the dioxane moiety.
(33) Croci, M. Single Molecule Spectroscopy. Ph.D. thesis, ETH Zürich Diss. No. 12186, 1997.
(34) Camerman, A.; Trotter, J. *Proc. R. Soc. London, Ser. A* **1964**, *279*, 129.
(35) Mandel, L.; Wolf, E. *Optical coherence and quantum optics*; Cambridge University Press: Cambridge, UK, 1995.
(36) Shalev, E.; Jortner, J. *Chem. Phys. Lett.* **1991**, *178*(1), 31−35.
(37) Moerner, W. E.; Plakhotnik, T.; Irngartinger, T.; Croci, M.; Palm, V.; Wild, U. P. *J. Phys. Chem.* **1994**, *98*(30), 7382−7389.
(38) Kohler, B. E.; Woehl, J. *J. Chem. Phys.* **1995**, *102*(20), 7773−7781.
(39) Vainer, Y. G.; Plakhotnik, T.; Personov, R. *Chem. Phys.* **1996**, *209*, 101−110.